NUMERICAL MODELLING OF UNSTABLE MODE I TRANSVERSE INTRALAMINAR CRACK PROPAGATION USING THE SIZE EFFECT LAW

Luís F. Varandas[1], Denis Dalli[2], Giuseppe Catalanotti[3] and Brian G. Falzon[4]

[1] Advanced Composite Research Group (ACRG), Queen's University Belfast, Belfast, UK,
Email: L.Varandas@qub.ac.uk, Web page: https://www.qub.ac.uk/sites/acrg/
[2] Advanced Composite Research Group (ACRG), Queen's University Belfast, Belfast, UK,
Email: ddalli01@qub.ac.uk, Web page: https://www.qub.ac.uk/sites/acrg/
[3] Advanced Composite Research Group (ACRG), Queen's University Belfast, Belfast, UK,
Email: G.Catalanotti@qub.ac.uk, Web page: https://www.qub.ac.uk/sites/acrg/
[4] Advanced Composite Research Group (ACRG), Queen's University Belfast, Belfast, UK,
Email: B.Falzon@qub.ac.uk, Web page: https://www.qub.ac.uk/sites/acrg/

Keywords: Polymer Matrix Composites (PMCs), Intralaminar fracture toughness, Size effect law, Computational Mechanics.

ABSTRACT

This paper presents a micromechanical Finite Element (FE) model to study mode I transverse intralaminar damage propagation in unidirectional (UD) composite materials. A computational framework consisting of Single Edge Notch Tension (SENT) virtual specimens, composed of Unit Cells (UCs) embedded in homogenised regions, is proposed. Random fibre distributions and appropriate constitutive models are used to model the different dissipative phenomena that occur at crack initiation and propagation. The corresponding crack-resistance curve (*R*-curve) is obtained by fitting the size effect law (SEL) to the peak loads obtained from geometrically scaled SENT FE models.

1 INTRODUCTION

For the prediction of damage propagation, state-of-the-art mesoscale (ply-level) computational damage models (e.g. [1, 2]) usually require the specification of fracture energy parameters associated to the main failure modes of unidirectional (UD) carbon fibre composite materials. Extensive experimental characterisation of both mode I and compressive intralaminar fracture toughness of UD composite materials has already been performed (e.g. [3, 4]). However, these have mostly been conducted for the longitudinal direction, i.e. in the direction of the fibrous reinforcements.

In the past, a number of authors have numerically analysed mode I transverse intralaminar crack propagation using a bi-dimensional (2D) framework (e.g. [5, 6]). However, the 2D nature of these analyses neglects some of the dissipation mechanisms, such as fibre bridging and out-of-plane matrix cracking. This creates a more brittle crack propagation scenario, where the calculated steady-state fracture toughness should be interpreted as an initiation value along the rising part of the R-curve, rather than a steady-state propagation value.

Experimental characterisation of the fracture toughness using the size effect method, proposed by Bažant [7], has also been adapted to UD composites. In terms of modelling, the unstable crack propagation specimens used for the size effect method possess a major advantage over stable specimen geometries. Since the peak load in unstable specimens occurs before the full development of the Fracture Process Zone (FPZ) at the crack tip, the detailed micromechanical region only needs to be as long as the FPZ of the material being investigated. Therefore, by making use of the appropriate constitutive material models [8], accounting for fibre distribution variability [9], this paper presents a three-dimensional (3D) numerical framework to characterise the mode I transverse intralaminar fracture toughness of UD composite materials, by means of the size effect method.

2 MICROMECHANICAL MODEL

2.1 Material models and properties

The epoxy matrix is modelled using the isotropic elastic-plastic constitutive damage model proposed by Melro et al. [8], implemented as a VUMAT user subroutine in the Finite Element (FE) commercial software Abaqus® [10]. The initial elastic behaviour is defined by a linear relation between the stress and elastic strain tensor. A paraboloidal yield criterion is used [11], defined as a function of the stress tensor and of the compressive and tensile yield strengths, together with a non-associative flow rule. A thermodynamically-consistent isotropic damage model is used, defined by a single damage variable, where damage onset is defined by the following damage activation function:

$$F_m^d = \phi_m^d - r_m = \frac{3\tilde{J}_2}{X_m^C X_m^T} + \frac{\tilde{I}_1(X_m^C - X_m^T)}{X_m^C X_m^T} - r_m \tag{1}$$

where ϕ_m^d is the loading function, X_m^C and X_m^T represent the compressive and tensile strengths of the epoxy, respectively, $\tilde{J}_2$ is the second invariant of the deviatoric effective stress tensor, $\tilde{I}_1$ is the first invariant of the effective stress tensor, and r_m is an internal variable.

To avoid mesh size dependency, Bažant and Oh's crack band model is employed [12]. This uses the individual characteristic element length and the mode I fracture toughness of the epoxy to regularise the computed dissipated energy. It is implemented along with the definition of a damage evolution law [8]. The dissipated energy is given by:

$$\Psi_{\mathrm{m}} = \int_0^\infty Y_m \, \dot{d}_m d_t = \int_1^\infty \frac{\partial \Pi_m}{\partial d_m} \frac{\partial d_m}{\partial r_m} dr_m = \frac{G_m^{Ic}}{l^e} \tag{2}$$

where Ψ_{m} is the energy dissipated per unit volume, Π_m is the complementary free energy density of the material, G_m^{Ic} is the mode I fracture toughness of the epoxy, and l^e is the characteristic finite element length.

The matrix damage variable, d_m, is defined as:

$$d_m = 1 - \frac{e^{A_m\left(3-\sqrt{7+2r_m^2}\right)}}{\sqrt{7+2r_m^2}-2} \tag{3}$$

where A_m is a parameter that needs to be computed for each matrix element of the FE mesh by solving Eq. (2) as a function of the characteristic element length, l^e. The Hexcel 8552 epoxy resin was considered here, with its elastic and strength properties obtained from Ref. [13] via nanoindentation experiments. The mode I fracture toughness is assumed to be an average value for Bisphenol-A type epoxies (e.g. [14]). Table 1 lists the mechanical properties considered to model the epoxy.

Since the main damage mechanisms associated with mode I transverse intralaminar crack propagation are mainly fibre-matrix interfacial debonding, and matrix plasticity and fracture, no non-linear or fracture behaviour is considered for the fibrous reinforcements. Therefore, they are assumed to have a linear-elastic transversely-isotropic behaviour. The fibres are assumed to have a fibre radius of $r_f = 3.5$ μm. Table 1 also presents the mechanical properties of standard AS4 carbon fibres.

The homogenised regions that surround the UC help reduce the computational cost of the simulations. Therefore, like the reinforcements, they are assumed to have a linear-elastic transversely-isotropic behaviour. Their elastic properties are obtained by making use of a separate micromechanical framework, composed of 3D Representative Volume Elements (RVEs), using a random dispersion

algorithm [15]. Following [16], the 3D RVEs are generated with admissible dimensions, and are subjected to 3D Periodic Boundary Conditions (PBCs) and to four different loading scenarios. The homogenised material properties in Table 1 are an average result of five RVE simulations, all having the same size and fibre volume fraction ($\omega_f^H = 56\%$), but with different random fibre distributions.

Mechanical property	Epoxy matrix [13]	AS4 fibres [17]	Homogenised parts
E_{11} [GPa]	5.07	22.5	131.0
E_{22} [GPa]	5.07	15.0	9.4
G_{12} [GPa]	1.88	15.0	5.2
G_{23} [GPa]	1.88	7.0	3.6
ν_{12}	0.35	0.2	0.3
X_m^T [MPa]	121	$--$	$--$
X_m^C [MPa]	180	$--$	$--$
G_m^{Ic} [N/mm]	0.09	$--$	$--$

Table 1: Mechanical properties of both constituents [13, 17] and homogenised parts.

2.2 Geometry and Boundary Conditions

The computational framework is composed of SENT virtual specimens, having a detailed micromechanical UC region, composed of 10 plies, each with different random fibre distributions [9], all having a fibre volume fraction of $\omega_f^{UC} = 56\%$. The total height of the UC is equal to $500\ \mu$m, ensuring that the triggered damage is only due to the presence of the crack, and not influenced by the surrounding homogenised regions. The specimen thickness is equal to $t = 0.75$ mm. A pre-crack is inserted by removing elements along the centreline of the virtual SENT specimens, with a height of approximately the in-plane dimensions of a single element of the UC mesh. Homogenised regions are attached to the UC through $Tie\ Constraints$. The total length of each FE specimen, encompassing the UC and both homogenised layers, is five times its total width, i.e. $2l = 5w$ [3]. Figure 1 shows a schematic representation of the model and applied Boundary Conditions (BCs).

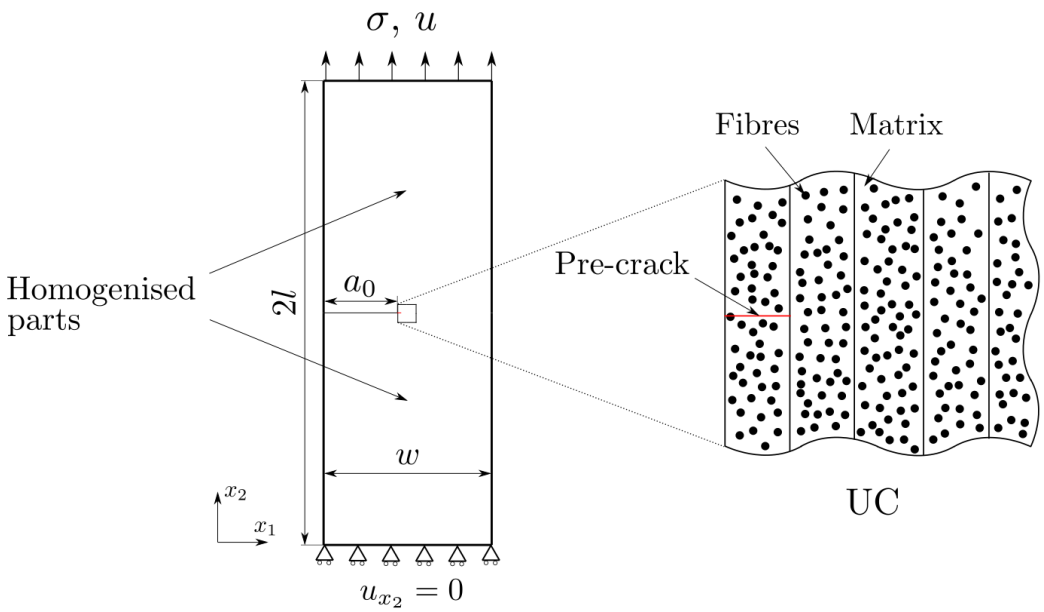

Figure 1: Schematic representation of the FE models and applied BCs.

All parts are modelled using 3D reduced integration hexahedral elements (C3D8R), with an average seed size of 1.2 μm. However, the homogenised parts have a biased seed size variation along their length, to reduce computational cost.

3 DETERMINATION OF THE CORRECTION FACTOR

An analytical model is used to obtain the mode I transverse intralaminar R-curve, using the recorded numerical peak loads for different sizes of virtual specimens, as proposed by Refs. [3, 4]. This model requires the determination of a correction factor, κ, which is obtained using the Virtual Crack Closure Technique (VCCT), in the FE commercial software Abaqus® [10]. One half of a 2D SENT specimen was generated, having the homogenised mechanical properties listed in Table 1. κ was calculated for various values of crack length to specimen width ratio, α, over the range $0 < \alpha < 1$. A polynomial fit of the numerical results was obtained for this correction factor:

$$\kappa = \sqrt{\tan\frac{\pi\alpha}{2}} \sum_i K_i \alpha^{i-1} \tag{4}$$

where K_i is a matrix of indices for a 2nd order fitting function for κ in terms of α [3, 4].

4 RESULTS

The mode I transverse intralaminar crack propagation was assessed by generating six virtual SENT FE models of different widths: $w = 2$ mm; 5 mm; 10 mm; 15 mm; 20 mm; 30 mm. Figure 2 shows the numerical predictions of the load-displacement curves for these different sized specimens, and the bilogarithmic size effect law fitting, $\sigma_u = \sigma_u(w)$, of the peak loads [7].

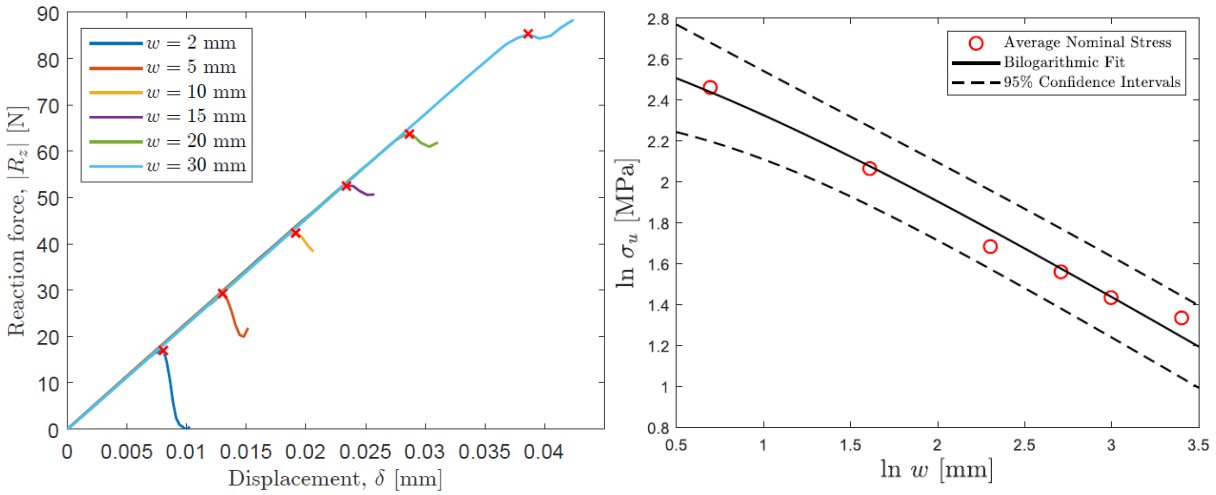

Figure 2: Numerical predictions of load-displacement for different virtual SENT specimen widths (left), and corresponding bilogarithmic size effect law of the peak loads, $\sigma_u = \sigma_u(w)$ (right).

As expected, Figure 2 (left) shows how the peak load increases with specimen size. However, this increase is not linearly proportional, indicating a size effect, observed in Figure 2 (right). In the post-peak response, after the crack has unstably propagated through the whole length of the UC, the homogenised parts are now carrying the load, justifying the rising part of the curve after initial instability. Figure 3 shows the contour plots of the matrix damage variable (Eq. (3)), at maximum applied displacement, for a virtual specimen of $w = 10$ mm. The damage, even after unstable fracture, is shown to be contained within close proximity of the developed crack.

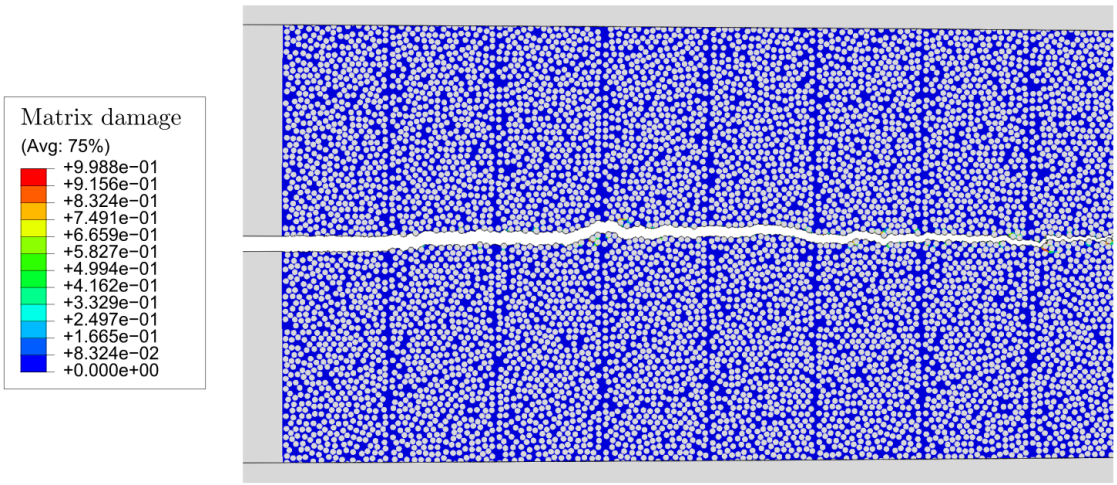

Figure 3: Contour plots of the matrix damage variable (Equation (3)) of a FE model having $w = 10$ mm.

The fracture toughness results obtained from the virtual SENT numerical models are presented in Figure 4. The driving force curves, $G_I(\Delta a)$, derived for different virtual specimen sizes (in blue), including those that were simulated using the computational framework (in red), were used to obtain the mode I transverse R-curve of the material (in black). The fully developed length of the FPZ, and the steady-state value of the fracture toughness, are respectively determined to be: $l_{FPZ} = 0.173$ mm and $R_{SS} = 0.207$ kJ/m^2.

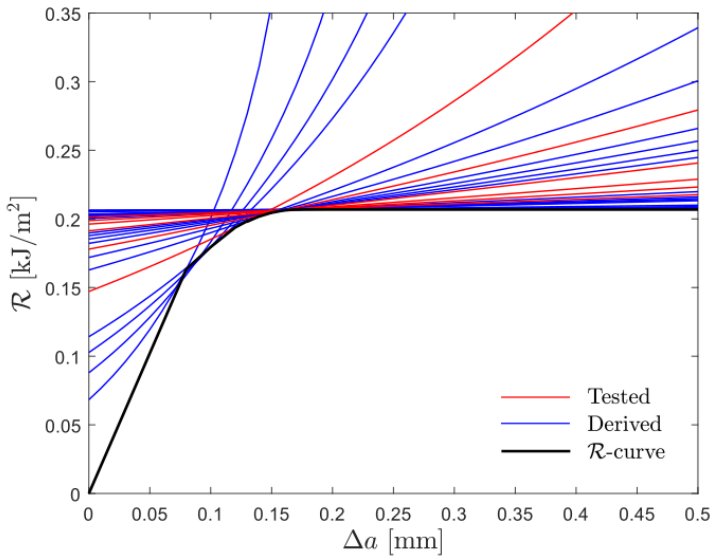

Figure 4: Numerical prediction of the R-curve (in black), and tested (in red) and derived (in blue) $G_I(\Delta a)$ curves.

It should be noted that the length of the fully developed FPZ and corresponding fracture toughness of the material, associated with a slit crack propagating in the transverse direction of a ply, are parameters which are not usually available in the literature due to the lack of available test methods. Thus, they are usually approximated as being equal to the mode I interlaminar values (usually obtained from a Double Cantilever Beam (DCB) test). Even if both these failure mechanisms involve fibre-matrix debonding and matrix degradation, interlaminar damage propagation is often characterised by fibre bridging, which influences the values obtained for both initial and steady-state R-curve parameters [19].

Here, the numerically predicted mode I steady-state fracture toughness is comparable with previous experimental values obtained for mode I interlaminar fracture toughness [20, 21]. However, several simplifications were made. Mechanical characterisation of the fibre-matrix interface is still a problematic challenge, especially the interfacial toughness. Therefore, a rigid contact was assumed between both constituents in the UC, leading to possible overestimations of the quantitative predictions of the peak loads. Therefore, to properly simulate the mechanical behaviour of the material, reliable mechanical properties for the matrix, and fibre-matrix interface are needed. Also, it has been reported that the matrix damage model used here must be further modified, to accurately dissipate the fracture energy being used in the analysis [22]. Finally, several virtual specimens should be simulated for each chosen size, with UCs that include different fibre distributions (while maintaining the fibre volume fraction constant), in order to assess microstructural randomness.

5 CONCLUSIONS AND FUTURE WORK

This work presented a microscale computational framework which is able to analyse unstable mode I transverse crack propagation in UD composite materials. Various sizes of virtual SENT specimens were generated and simulated, to numerically predict their respective peak loads. Using an analytical method developed by Refs. [3, 4] and the size effect law [7], these peak loads were subsequently used to determine the mode I transverse fracture toughness of the material.

Future developments of this framework will include the addition of interface regions, performing the aforementioned modifications to the matrix damage model, studying the sensitivity of the peak load to the pre-crack tip radius (as done experimentally by Refs. [23, 24]); and the sensitivity of the UC size and fibre volume fraction on the numerical predictions of the fracture toughness of the material.

ACKNOWLEDGEMENTS

The authors gratefully acknowledge the financial support of the project ICONIC – Improving the crashworthiness of composite transportation structures. ICONIC has received funding from the European Union's Horizon 2020 research and innovation programme under the Marie Skłodowska-Curie grant agreement No 721256. The content reflects only the authors' view and the Agency is not responsible for any use that may be made of the information it contains.

REFERENCES

[1] P. Maimí, P.P. Camanho, J.A. Mayugo and C.G. Dávilla. A continuum damage model for composite laminates: Part 1 – Constitutive model, *Mech. Materials*, **39**, 2007, pp. 897-908 (doi.org/10.1016/j.mechmat.2007.03.005).

[2] W. Tan, B.G. Falzon and M. Price. Predicting the crushing behaviour of composite material using high-fidelity finite element modelling, *Int. Journ. Of Crash.*, **20**, 2015, pp. 60-77 (doi.org/10.1080/13588265.2014.972122).

[3] G. Catalanotti, J. Xavier and P.P. Camanho. Measurement of the compressive crack resistance curve of composites using the size effect law, *Comp. Part A: Manuf.*, ***56***, 2014, pp. 300-307 (doi.org/10.1016/j.compositesa.2013.10.017).

[4] G. Catalanotti, A. Arteiro, M. Hayati and P.P. Camanho. Determination of the mode I crack resistance curve of polymer composites using the size-effect law, *Eng. Frac. Mech.*, **118**, 2014, pp. 49-65 (doi.org/10.1016/j.engfracmech.2013.10.021).

[5] D.J. Mortell, D.A. Tanner and C.T. McCarthy. A virtual experimental approach to microscale composites testing, *Composite Structures*, **171**, 2017, pp. 1-9 (doi.org/10.1016/j.compstruct.2017.03.016).

[6] M. Herráez, C. González and C.S. Lopes. A numerical framework to analyze fracture in composite materials: From R-curves to homogenized softening laws, *Int. Jour. of Sold. and Struc.*, **134**, 2018, pp. 216-228 (doi.org/10.1016/j.ijsolstr.2017.10.031).

[7] Z.P. Bažant and J. Planas, *Fracture and Size Effect in Concrete and Other Quasibrittle Materials*, CRC Press, 1998.

[8] A.R. Melro, P.P. Camanho, F.M. Andrade Pires and S.T. Pinho. Micromechanical analysis of polymer composites reinforced by unidirectional fibres: Part I – Constitutive modelling, *Int. Jour. of Sold. and Struc.*, **50**, 2013, pp. 1897-1905 (doi.org/10.1016/j.ijsolstr.2013.02.009).

[9] L.F. Varandas, A. Arteiro, M.A. Bessa, A.R. Melro and G. Catalanotti. The effect of through-thickness compressive stress on mode II interlaminar crack propagation: A computational micromechanics approach, *Composite Structures*, **182**, 2017, pp. 326-334 (doi.org/10.1016/j.compstruct.2017.09.020).

[10] Dassault Systèmes, Providence, RI, USA. *Abaqus Documentation*.

[11] N.W. Tschoegl. Failure surfaces in principal stress space, *J. Polym. Sci. Part C: Polym Symposia*, **32**, 1971, pp. 239-267 (doi.org/10.1002/polc.5070320113).

[12] Z.P. Bažant and B.H. Oh. Crack band theory for fracture of concrete, *Materials and Structures.*, **16**, 1983, pp. 155-177 (doi.org/10.1007/BF02486267).

[13] F. Naya, C. González, C.S. Lopes, S. Van der Veen and F. Pons. Computational micromechanics of the transverse and shear behavior of unidirectional fiber reinforced polymers including environmental effects, *Comp. Part A: Manuf.*, **92**, 2017, pp. 146-157 (doi.org/10.1016/j.compositesa.2016.06.018).

[14] T.H. Hsieh, A.J. Kinloch, K. Masania, A.C. Taylor and S. Sprenger. The mechanisms and mechanics of the toughening of epoxy polymers modified with silica nanoparticles, *Polymer*, **51**, 2010, pp. 6284-6294 (doi.org/10.1016/j.polymer.2010.10.048).

[15] G. Catalanotti. On the generation of RVE-based models of composites reinforced with long fibres or spherical particles, *Composite Structures*, **138**, 2016, pp. 84-95 (doi.org/10.1016/j.compstruct.2015.11.039).

[16] A.R. Melro, P.P. Camanho and S.T. Pinho. Influence of geometrical parameters on the elastic response of unidirectional composite materials, *Composite Structures*, **94**, 2012, pp. 3223-3231 (doi.org/10.1016/j.compstruct.2012.05.004).

[17] P.D. Soden, M.J. Hinton, A.S. Kaddour. Lamina properties, lay-up configurations and loading conditions for a range of fibre-reinforced composite laminates, *Comp. Sci. and Tech.*, **58**, 1998, pp. 1011-1022 (doi.org/10.1016/S0266-3538(98)00078-5).

[18] M.L. Benzeggagh and M. Kenane. Measurement of mixed-mode delamination fracture toughness of unidirectional glass/epoxy composites with mixed-mode bending apparatus, *Comp. Sci. and Tech.*, **56**, 1996, pp. 439-449 (doi.org/10.1016/0266-3538(96)00005-X).

[19] G. Catalanotti. Prediction of in situ strengths in composites: Some considerations, *Composite Structures.*, **207**, 2019, pp. 889-893 (doi.org/10.1016/j.compstruct.2018.09.075).

[20] P.P. Camanho, C.G. Dávila, S.T. Pinho, L. Iannucci and P. Robinson. Prediction of in situ strengths and matrix cracking in composites under transverse tension and in-plane shear, *Comp. Part A: Manuf.*, **37**, 2006, pp. 165-176 (doi.org/10.1016/j.compositesa.2005.04.023).

[21] B.G. Falzon, S.C. Hawkins, C.P. Huynh, R. Radjef and C. Brown. An investigation of Mode I and Mode II fracture toughness enhancement using aligned carbon nanotubes forests at the crack interface, *Composite Structures.*, **106**, 2013, pp. 65-73 (doi.org/10.1016/j.compstruct.2013.05.051).

[22] A. Arefi, F.P. van der Meer, M.R. Forouzan and M. Silani. Formulation of a consistent pressure-dependent damage model with fracture energy as input, *Composite Structures.*, **201**, 2018, pp. 208-216 (doi.org/10.1016/j.compstruct.2018.06.005).

[23] M.J. Laffan, S.T. Pinho, P. Robinson and A.J. McMillan. Translaminar fracture toughness: The critical notch tip radius of 0° plies in CFRP, *Comp. Sci. and Tech.*, **72**, 2018, pp. 97-102 (doi.org/10.1016/j.compscitech.2011.10.006).

[24] D. Dalli, G. Catalanotti, L.F. Varandas, B.G. Falzon and S. Foster. Mode I intralaminar fracture toughness of 2D woven carbon fibre reinforced composites: A comparison of stable and unstable crack propagation techniques, *Eng. Frac. Mech.*, **214**, 2019, pp. 427-448 (doi.org/10.1016/j.engfracmech.2019.04.003).